Available online at www.sciencedirect.com
ScienceDirect
Earth and Planetary Science Letters 253 (2007) 389–401
EPSL
www.elsevier.com/locate/epsl

High and dry in central Tibet during the Late Oligocene

Peter G. DeCelles [a,*], Jay Quade [a], Paul Kapp [a], Majie Fan [a], David L. Dettman [a], Lin Ding [b]

[a] Department of Geosciences, University of Arizona, Tucson, Arizona 85721, United States
[b] Institute of Tibetan Plateau Research, Chinese Academy of Sciences, Beijing 100029, People's Republic of China

Received 12 July 2006; received in revised form 1 November 2006; accepted 1 November 2006
Available online 8 December 2006
Editor: M.L. Delaney

Abstract

The time at which the Tibetan Plateau rose to its present high elevation remains controversial, with estimates ranging from 40 Ma to more recent than 7 Ma. New stable isotope analyses of modern and accurately dated ancient paleosol carbonate in the Nima basin of central Tibet point to an arid climate and high paleoelevation (4.5–5 km, comparable to today's setting) by 26 Ma. Oxygen isotope values of ancient (26 Ma) soil carbonate are both very negative and indistinguishable–after modest corrections for changes in global climate–from the lowest (least evaporated) oxygen isotope values of modern soil carbonates in the area. Substantial enrichments in oxygen-18 in paleolacustrine carbonates, as well as high carbon isotope values from paleosol carbonates, indicate considerable lake evaporation and low soil respiration rates, respectively, and both are consistent with the present arid climate of the Nima area. Blockage of tropical moisture by the Himalaya and perhaps the Gangdese Shan probably has contributed strongly to the aridity and very negative oxygen isotope values of soil carbonate and surface water in the Nima area since at least the Late Oligocene. The maintenance of high elevation since at least 26 Ma suggests that any flow of lower crust from beneath central Tibet must have been balanced by coeval northward insertion of Indian crust beneath the Plateau.

Keywords: Tibet; Paleoelevation; Continental tectonics; Carbon isotopes; Oxygen isotopes

1. Introduction

The timing of attainment of regional high elevation (4 to 5 km) in the Tibetan Plateau (Fig. 1) is a significant problem in continental tectonics because elevation strongly influences the force distribution in and adjacent to orogenic plateaux [1,2], and the timing and mechanisms of elevation gain are important in competing general models of plateau formation (compare [1–8]) and global and regional climate change [9–11]. Our knowledge of the uplift history of the Tibetan Plateau remains poor, however, because of the scarcity of well-dated ancient sediments containing unambiguous indicators of paleoelevation. The pursuit of paleoaltimetry data from Tibet is motivated in part by the need to better constrain the initial development of high elevation in this region as a means of testing tectonic models for Tibet. For example, models that infer uplift of the Plateau in response to removal of a convective instability in the upper mantle call for rapid, regional uplift during Late Miocene time [1], whereas models that build the Plateau by addition of

* Corresponding author. Tel.: +1 520 621 4910; fax: +1 520 621 2672.
E-mail address: decelles@geo.arizona.edu (P.G. DeCelles).

0012-821X/$ - see front matter © 2006 Elsevier B.V. All rights reserved.
doi:10.1016/j.epsl.2006.11.001

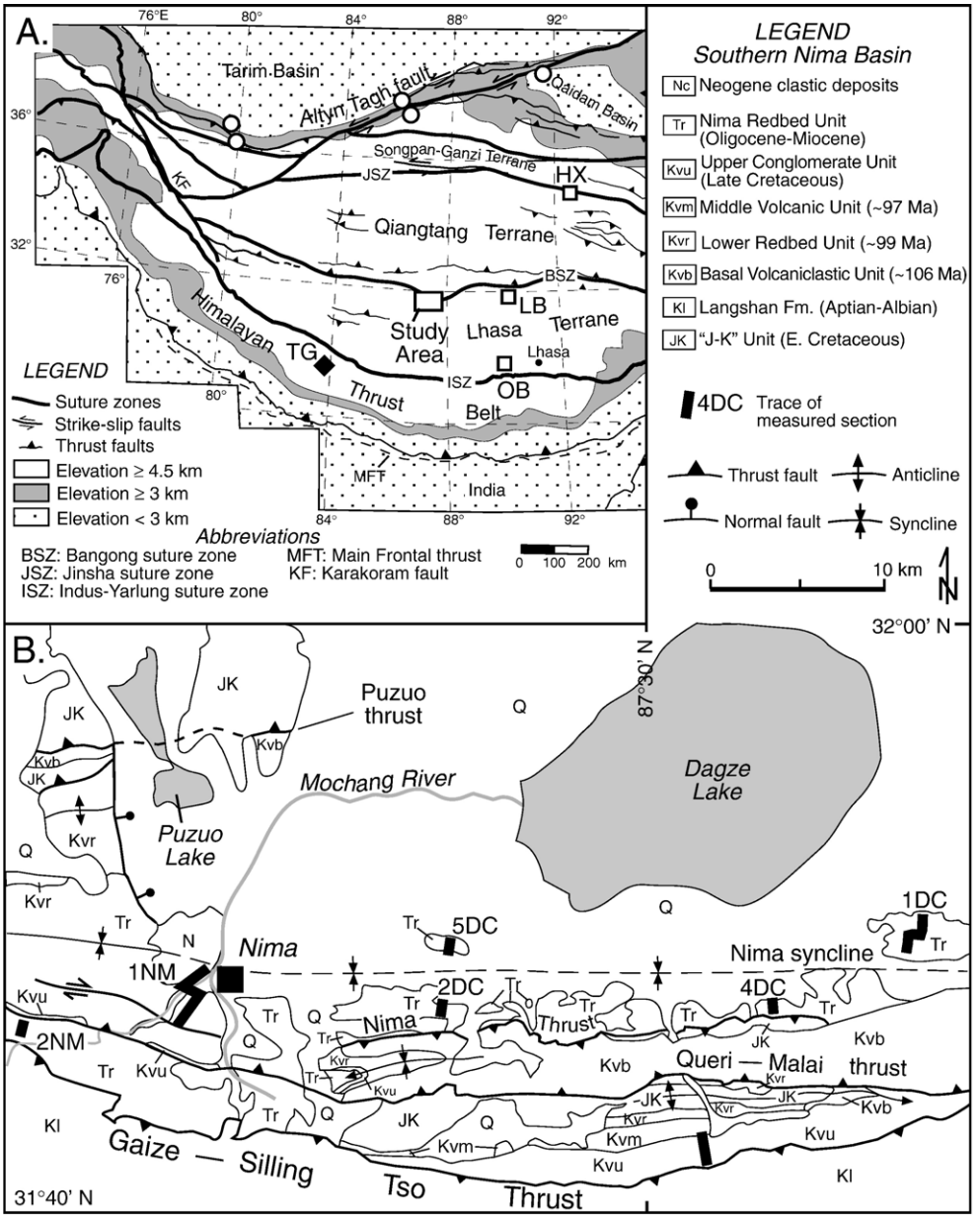

Fig. 1. (A) Elevation and generalized tectonic map of the Tibetan Plateau. Open squares represent localities in Oiyug basin (OB), Lunpola basin (LB), and Hoh Xil (HX), as reported in [21–23]. Open circles represent sampled localities reported in [24]. Filled diamond in central Himalaya shows location of samples collected in Thakkhola graben (TG) reported by [13,14]. (B) Geological map of the southern portion of the Nima basin, showing locations of measured sections. Samples for this study were collected primarily from section 4DC (see Fig. 3). Tuffs were sampled in sections 1DC, 2DC, and 2NM.

Indian crustal material from the south predict a progressive northward increase of elevation from Late Eocene time onward [3,7,8]. Other models call for gravitationally driven north- and northeastward expansion of the Plateau by ductile flow of lower to middle crustal material [2,5], a process that demands an explanation for the origin of thick crust in central Tibet at the onset of crustal flow.

Oxygen isotopic values from carbonates (expressed as $\delta^{18}O_{cc}$ in ‰) and the waters from which they precipitate ($\delta^{18}O_{mw}$) decrease with increasing elevation, making them potentially useful paleoaltimeters. Ancient carbonates in the geologic record have been analyzed as paleoelevation indicators in a variety of orogenic belts [12–26]. Paleobotanic [27] and oxygen isotopic data from southern Tibet suggest that high (>4 km)

paleoelevations were attained at Thakkhola [14] and in the Oiyug Basin [22] (Fig. 1) by the Middle to Late Miocene (roughly 15–10 Ma). The picture is less clear further back in the geologic record. Oxygen isotopic analysis of carbonates from Hoh Xil in northern Tibet (Fig. 1) suggests that paleoelevation during the Late Eocene was ~ 2000 m, significantly lower than the modern elevation of 4700–5300 m in this region [21]. This reconstruction of paleoelevation depends critically on the choice of isotopic lapse rate, which differs dramatically between northern and southern Tibet. In the Hoh Xil study, modern $\delta^{18}O_{mw}$ versus elevation relationships established in the distant Nepalese Himalaya [13,18,30] – where monsoon-dominated isotopic lapse rates are very steep – were used to reconstruct paleoelevation [21], instead of the more modest lapse rates characteristic of northern Tibet (encompassing Xoh Xil) today. In fact, reconstructed $\delta^{18}O_{mw}$ values from Hoh Xil are very similar to $\delta^{18}O_{mw}$ values of modern precipitation in the northern Tibetan Plateau, which is derived from recycled continental moisture with $\delta^{18}O$ (SMOW) values of −9‰ to −10‰ [28,29]. The use of the gentler lapse rate currently in place for northern Tibet implies that elevation has not changed substantially in this region since the Late Eocene.

At Lunpola basin in central Tibet (Fig. 1), isotopic evidence points to Late Eocene paleoelevations comparable to the present ~ 4500 m elevation [23]. However, the age of the Lunpola basin deposits is based on palynological biozonation without geochronological control (see [23]). In general, age control is lacking for putative Cenozoic deposits in the Plateau interior, and adjacent successions of lithologically similar nonmarine deposits can range in age from Early Cretaceous to Miocene. Previous age assignments based largely on biostratigraphy and lithostratigraphic correlation are highly suspect (e.g., [30,31]). Coupled with the potential underestimates of Eocene paleoelevation at Hoh Xil discussed above, the imprecise age control on the Lunpola basin deposits raises concern about the inference of progressive northward growth of the Tibetan Plateau from Eocene time forward during the Indo–Asian collision [21,23,32]. Adding to the complexity of Tibetan paleoelevation records during the Cenozoic are data from a large sector of the northern margin of the Plateau, which indicate a major positive shift in $\delta^{18}O$ values from Eocene to Oligocene time [24]. This isotopic shift north of the Tibetan Plateau was interpreted to result from climate change associated with the rise of the Tibetan–Himalayan region to high elevations [24].

What is clearly needed are isotopic analyses of carbonates from well-dated basins situated within the interior of the Tibetan Plateau, and $\delta^{18}O_{mw}$ values of locally sampled, modern waters and soils in order to calibrate the relationship between $\delta^{18}O_{cc}$ and paleoelevation. In this paper we focus on modern and radiometrically dated ancient paleosol carbonates, ancient lacustrine marl deposits and fossils, and modern stream waters and soil carbonates collected in the Nima basin area in the heart of the Tibetan Plateau at elevations of 4500–4700 m. We show that paleoelevation at ~ 26 Ma in this region was not significantly different from modern elevation, which in turn provides strong constraints on tectonic models for the formation of the Tibetan Plateau. In particular, models that call for regional uplift of Tibet during Late Miocene time may need to be revised.

2. Setting of Nima Basin

Nima basin is located ~ 240 km west of the Lunpola basin and ~ 450 km northwest of Lhasa (Fig. 1). Like the Lunpola basin, the Nima basin is located in the southern part of the Bangong suture zone, which separates the Qiangtang and Lhasa terranes in central Tibet (Fig. 1). From mid-Cretaceous through Late Miocene time a variety of nonmarine deposits accumulated in the Nima basin, derived from high, thrust-fault-bounded ranges to the south and north that were uplifted during reactivation of the Bangong suture owing to continued convergence between the Lhasa and Qiangtang terranes after they had collided during Early Cretaceous time [6,30]. The southern Nima basin contains more than 4 km of Tertiary alluvial, fluvial,

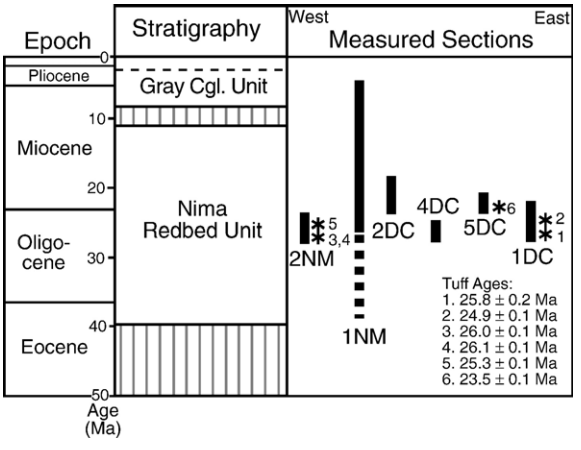

Fig. 2. Chronostratigraphic chart of the southern Nima basin showing the distribution and correlation of measured sections in the Nima Redbed unit and locations of dated tuff samples. See Fig. 1 for locations of measured sections.

lacustrine, and lacustrine fan-delta deposits that accumulated in close proximity to growing thrust-faulted ranges [33]. Detailed geological maps and stratigraphic sections of the Nima basin are presented in [34] and [35]. Lacustrine marl beds and well-developed Calcisols (paleosols with abundant pedogenic carbonate nodules) are common in the informally designated Nima Redbed unit (Figs. 1, 2), which is exposed in a roughly 50 km long outcrop belt along the southern margin of the Nima basin in the proximal footwall of the Nima thrust fault (Fig. 1).

3. Geochronology

For age control, $^{40}Ar/^{39}Ar$ geochronology on biotite separates from samples of six reworked tuffs in the Nima Redbed unit securely places the age of the analyzed deposits between 25 and 26 Ma (Late Oligocene; Fig. 2). $^{40}Ar/^{39}Ar$ ages on biotites were determined by M. Heizler at the New Mexico Geochronology Research Laboratory. Single-crystal laser and step-heating age results are summarized in [34]. The tuffs consist of fine-grained sand, silt, and abundant coarse-grained, euhedral, pseudo-hexagonal biotite crystals. Lithofacies indicate that the tuffs were deposited in shallow ponds and lakes and subsequently were mixed with terrigenous clastic sediments. Biotite ages from six tuffaceous horizons range from 26.1±0.1 Ma to 23.5±0.1 Ma (1σ) (Fig. 2). Our stable isotopic analyses were conducted on samples at the same stratigraphic levels as the 26–25 Ma tuffs and stratigraphically below the ~ 23.5 Ma tuff (Figs. 2, 3).

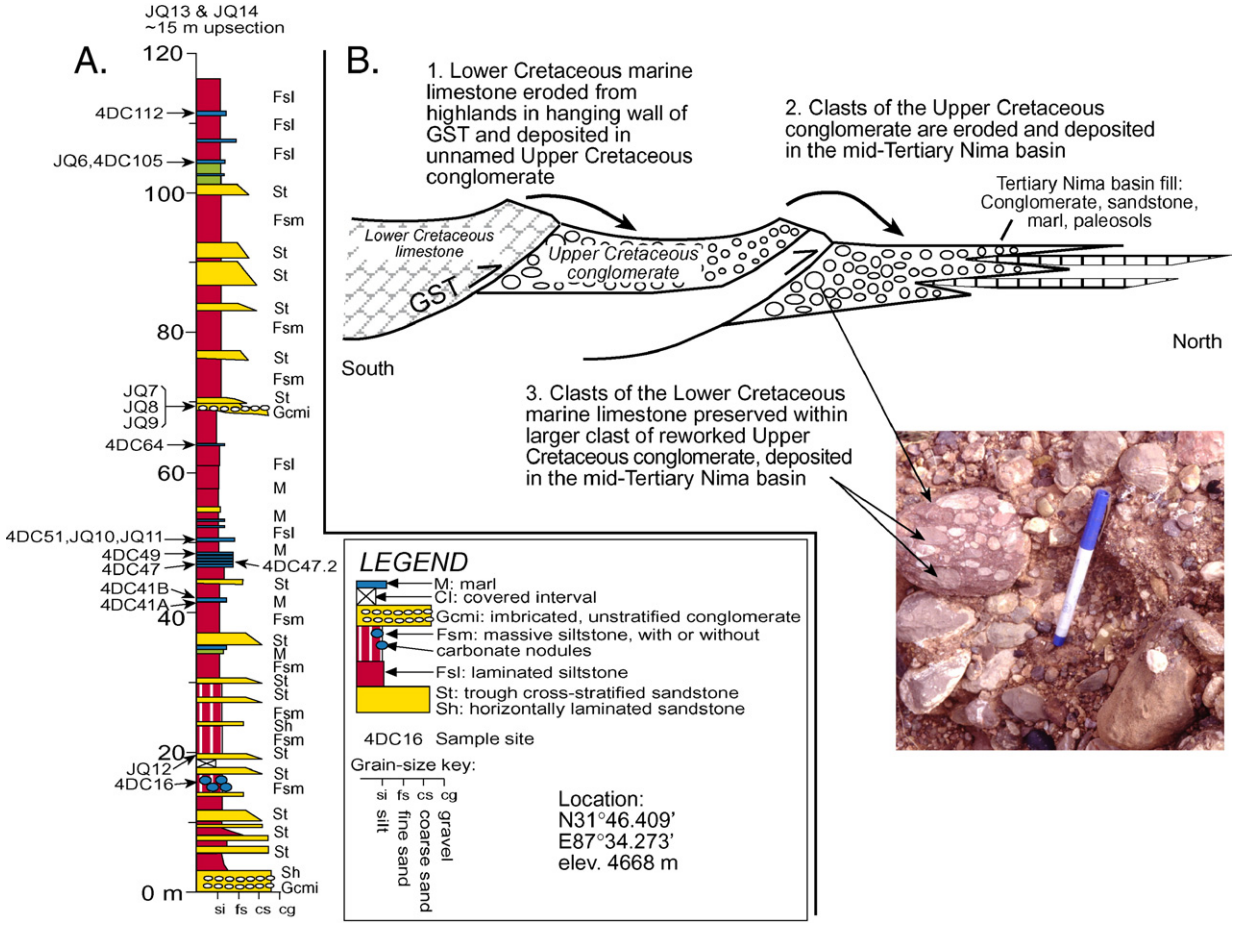

Fig. 3. (A) Stratigraphic section 4DC from which most of the samples reported here were collected (see Fig. 1 for location, and Fig. 2 for chronostratigraphic context). (B) Schematic diagram illustrating the sequence of events that led to the deposition of marine limestone clasts analyzed in this study: (1) clasts of Lower Cretaceous marine limestone are eroded from highlands in hanging wall of the Gaize-Silling Tso thrust (GST) and deposited in the unnamed Upper Cretaceous conglomerate. (2) Clasts of the Upper Cretaceous conglomerate, including pebbles of the previously deposited Lower Cretaceous marine limestone, are eroded and deposited in the mid-Tertiary Nima basin, along with paleosol carbonate and lacustrine marl. The section illustrated in (A) is located in the Nima basin fill.

4. Approach and methods

Key questions for paleoelevation reconstructions using oxygen isotopes include (1) the sensitivity, past and present, of $\delta^{18}O_{cc}$ values to elevation; (2) whether burial in deep sedimentary basins has led to diagenetic alteration of primary $\delta^{18}O_{cc}$ values; and (3) whether evaporation has increased the $\delta^{18}O_{mw}$ values of paleowaters, and therefore also the values of carbonates precipitated from those waters, producing underestimates of paleoelevation. In this paper, we take a fresh approach to these questions by presenting data from modern surficial carbonates in the study region, using both the oxygen and carbon isotopic systems, combined with a novel approach to assessing potential diagenetic effects in ancient carbonates. Oxygen and stable carbon isotopic analyses were conducted on reworked and *in situ* Tertiary paleosol carbonate nodules, lacustrine marls, and calcareous fossils, and on reworked clasts of Lower Cretaceous (~ 115–105 Ma) Langshan Formation marine limestone in the Nima basin deposits. We also use carbon isotopes from modern soils and paleosols to assess aridity in the past, providing an additional tool for evaluating regional elevation insofar as current aridity in Tibet is produced by orographic blockage of monsoonal moisture from the south [36].

In order to assess the potential for diagenetic resetting of the isotopic paleoelevation signal [37], we employed an "isotopic conglomerate test" analogous to a standard technique in paleomagnetic studies used to evaluate potential secondary remagnetization of original paleomagnetic signals [38]. We analyzed limestone clasts in cobbles of reworked conglomerate that were recycled at least twice from the Lower Cretaceous Langshan Formation marine limestone and ultimately were

Table 1
Analyses of in situ and reworked paleosol carbonate nodules from section shown in Fig. 3

Sample #	Raw		Corrected				Description
	$\delta^{13}C$	$\delta^{13}O$	$\delta^{13}C$	$\delta^{13}O$	GPS location		
	PDB	PDB	PDB	PDB	Longitude	Latitude	
4DC16-5	−3.7	−16.9	−2.9	−14.4	45R 0554010	3515476	In situ paleosol nodule
4DC16-6	−2.9	−16.9	−2.2	−14.4	45R 0554010	3515476	In situ paleosol nodule
4DC16-7	−4.4	−16.8	−3.7	−14.3	45R 0554010	3515476	In situ paleosol nodule
4DC16-8	−4.4	−17.1	−3.7	−14.6	45R 0554010	3515476	In situ paleosol nodule
4DC16-9	−2.3	−16.9	−1.5	−14.4	45R 0554010	3515476	In situ paleosol nodule
4DC16-1	−2.8	−17.0	−2.1	−14.5	45R 0554010	3515476	In situ paleosol nodule
4DC16-3	−3.8	−16.4	−3.0	−13.9	45R 0554010	3515476	In situ paleosol nodule
JQ12C-3	−2.9	−17.1	−2.2	−14.6	45R 0554010	3515476	In situ paleosol nodule
JQ12C-4	−3.8	−17.1	−3.1	−14.6	45R 0554010	3515476	In situ paleosol nodule
4DC16-1	−2.8	−17.0	−2.1	−14.5	45R 0554010	3515476	In situ paleosol nodule
4DC16-3	−3.8	−16.4	−3.0	−13.9	45R 0554010	3515476	In situ paleosol nodule
4DC16-4	−3.3	−17.2	−2.6	−14.7	45R 0554010	3515476	In situ paleosol nodule
4DC16/11	−3.7	−16.9	−3.0	−14.4	45R 0554010	3515476	In situ paleosol nodule
4DC16/13	−3.8	−16.8	−3.1	−14.3	45R 0554010	3515476	In situ paleosol nodule
JQ12C-1	−4.0	−17.4	−3.3	−14.9	45R 0554010	3515476	In situ paleosol nodule
JQ12C-4	−3.9	−17.2	−3.2	−14.7	45R 0554010	3515476	In situ paleosol nodule
JQ12C-5	−3.8	−17.5	−3.1	−15.0	45R 0554010	3515476	In situ paleosol nodule
JQ12C B	−3.6	−17.1	−2.9	−14.6	45R 0554010	3515476	In situ paleosol nodule
JQ12C C	−4.6	−17.3	−3.9	−14.8	45R 0554010	3515476	In situ paleosol nodule
JQ12C D	−3.7	−17.4	−2.9	−14.9	45R 0554010	3515476	In situ paleosol nodule
JQ12C F	−3.4	−16.6	−2.7	−14.1	45R 0554010	3515476	In situ paleosol nodule
JQ12A1	−2.6	−16.5	−1.9	−14.0	45R 0554010	3515476	Reworked paleosol nodule
JQ12A1-2	−2.9	−16.8	−2.2	−14.3	45R 0554010	3515476	Reworked paleosol nodule
JQ12A1-4	−3.1	−16.4	−2.4	−13.9	45R 0554010	3515476	Reworked paleosol nodule
JQ12A1-5	−3.6	−17.5	−2.9	−15.0	45R 0554010	3515476	Reworked paleosol nodule
JQ12A1-6	−3.5	−17.3	−2.8	−14.8	45R 0554010	3515476	Reworked paleosol nodule
JQ12A1-7	−3.3	−16.5	−2.6	−14.0	45R 0554010	3515476	Reworked paleosol nodule
JQ12A2-1	−4.6	−17.1	−3.9	−14.6	45R 0554010	3515476	Reworked paleosol nodule
JQ12A2-3	−4.0	−16.9	−3.3	−14.4	45R 0554010	3515476	Reworked paleosol nodule
JQ12A2-4	−3.6	−16.6	−2.9	−14.1	45R 0554010	3515476	Reworked paleosol nodule
JQ12A2-5	−4.2	−16.3	−3.5	−13.8	45R 0554010	3515476	Reworked paleosol nodule
Average	−3.5	−17.0	−2.9	−14.4			
Standard Deviation	0.6	0.3	0.6	0.3			

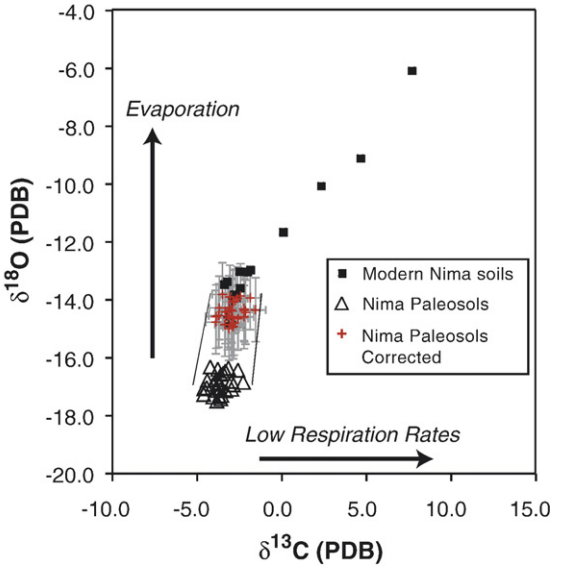

Fig. 4. $\delta^{18}O_{cc}$ (PDB) versus $\delta^{13}C_{cc}$ (PDB) of modern soil carbonate compared to both corrected and uncorrected (raw) values from Nima basin paleosol carbonates. Corrections made to isotope values of paleosol carbonates are discussed in text. Error bars on the corrected soil carbonate values reflect uncertainties in the paleotemperature estimate of ±5 °C.

deposited, along with locally reworked paleosol carbonate nodules, in Nima basin fluvial channels during Late Oligocene time (Fig. 3). The marine limestone is in the hanging wall of the Gaize-Silling Tso thrust fault (Fig. 1), which provided much of the Tertiary sediment that fills the southern Nima basin [35]. Clasts of limestone were eroded during the Late Cretaceous and deposited in a thick succession of coarse-grained Upper Cretaceous conglomerate along the southern fringe of the Nima basin (the Upper Conglomerate Unit in Fig. 1). During middle Tertiary time, this Upper Cretaceous conglomerate was uplifted and partly recycled into the Tertiary deposits of the Nima basin. Recycled clasts of the Upper Cretaceous conglomerate commonly contain pebbles of the Lower Cretaceous marine limestone (Fig. 3). The Nima basin also contains *in situ* lacustrine marl and argillic Calcisols [39], and these deposits were locally reworked into conglomeratic fluvial channel deposits, along with clasts of the Lower Cretaceous marine limestone and reworked clasts of the Upper Cretaceous conglomerate (Fig. 3). Therefore, if resetting by diagenesis has occurred in the Nima basin, carbonates of all types should exhibit similar and generally very negative $\delta^{18}O_{cc}$ values, and clasts of Lower Cretaceous marine limestone should not retain their primary marine $\delta^{18}O_{cc}$ values owing to diagenetic interaction with isotopically very negative meteoric water that is characteristic of recharge in the region today.

Samples of paleosol carbonate and marl were collected from detailed measured sections in the southern part of Nima basin (Fig. 3; Table 1). We also analyzed well-preserved samples of gastropods, ostracodes, and *Chara* in micritic marl beds. Pedogenic carbonate nodules were broken to reveal their internal structure and to avoid analysis of any nonpedogenic spar in vugs and small veinlets. Thin sections were studied to locate areas of pristine micritic carbonate, which were microsampled under a binocular microscope with a 0.5 mm drill bit at 2 mm intervals along an interior cross-section. All carbonate samples were heated at 150 °C for 3 h *in vacuo* and processed using an automated sample preparation device (Kiel III) attached directly to a Finnigan MAT 252 mass spectrometer at the University of Arizona. $\delta^{18}O$ and $\delta^{13}C$ values were normalized to NBS-19 based on internal lab standards. Precision of repeated standards is ±0.1‰ for $\delta^{18}O$ and ±0.06‰ for $\delta^{13}C$ (1σ).

The $\delta^{18}O_{cc}$ values of paleosol carbonates must be adjusted in order to compare with modern $\delta^{18}O_{cc}$ values of soil carbonate from the area. Soil carbonates from south of the Himalaya (the source region for most southern and central Tibetan rainfall today [29]) were 2–3‰ lower in $\delta^{18}O_{cc}$ values during the Early Miocene, a

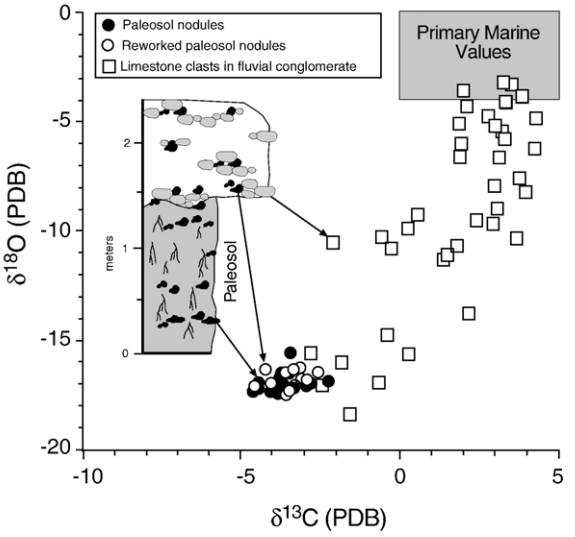

Fig. 5. $\delta^{18}O$ (PDB) versus $\delta^{13}C$ (PDB) of carbonates from Nima basin. Carbonate nodules were sampled *in situ* from buried paleosol shown in measured section format on the left, and from stratigraphically overlying reworked Oligocene channel deposits, where nodules (black pebbles in diagram) are mixed with clasts of Cretaceous limestone (light gray pebbles in diagram). Clasts of limestone come from both this outcrop and from three other conglomerates in the section. Gray box defining primary marine isotopic values for the mid-Cretaceous is from [44].

Table 2
Analyses of reworked Cretaceous marine limestone clasts in Nima basin

Sample #	$\delta^{13}C$ PDB	$\delta^{18}O$ PDB	Description	GPS location	
				Longitude	Latitude
2A1/NIMA	3.3	−5.8	Limestone clast	45R 0537714	3515090
2A2/NIMA	3.2	−5.5	Limestone clast	45R 0537714	3515090
2A3/NIMA	3.3	−3.2	Limestone clast	45R 0537714	3515090
2A4/NIMA	3.3	−4.1	Limestone clast	45R 0537714	3515090
2A5/NIMA	3.5	−3.3	Limestone clast	45R 0537714	3515090
2B1/NIMA	1.9	−5.1	Limestone clast	45R 0537714	3515090
2B2/NIMA	3.0	−5.2	Limestone clast	45R 0537714	3515090
2B4/NIMA	3.0	−7.9	Limestone clast	45R 0537714	3515090
2C3/NIMA	1.5	−11.1	Limestone clast	45R 0537714	3515090
2C4/NIMA	2.9	−9.7	Limestone clast	45R 0537714	3515090
2C5/NIMA	−2.1	−10.5	Limestone clast	45R 0537714	3515090
2C6/NIMA	3.8	−7.6	Limestone clast	45R 0537714	3515090
2C7A/NIMA	1.8	−10.7	Limestone clast	45R 0537714	3515090
2C7B/NIMA	1.4	−11.4	Limestone clast	45R 0537714	3515090
2D/NIMA	2.5	−5.9	Limestone clast	45R 0537714	3515090
2E/NIMA	1.9	−6.6	Limestone clast	45R 0537714	3515090
2F/NIMA	3.9	−8.2	Limestone clast	45R 0537714	3515090
2G/NIMA	3.8	−3.8	Limestone clast	45R 0537714	3515090
2H/NIMA	3.1	−6.6	Limestone clast	45R 0537714	3515090
2I/NIMA	2.4	−9.6	Limestone clast	45R 0537714	3515090
2J/NIMA	3.7	−10.4	Limestone clast	45R 0537714	3515090
7A/NIMA	−0.6	−10.3	Limestone clast	Section 4DC	
7B/NIMA	2.1	−4.4	Limestone clast	Section 4DC	
7C/NIMA	4.3	−4.8	Limestone clast	Section 4DC	
7D/NIMA	0.6	−9.3	Limestone clast	Section 4DC	
7F/NIMA	2.2	−13.8	Limestone clast	Section 4DC	
7G/NIMA	2.0	−3.6	Limestone clast	Section 4DC	
7H/NIMA	2.8	−4.7	Limestone clast	Section 4DC	
7I/NIMA	3.0	−9.0	Limestone clast	Section 4DC	
7J/NIMA	4.3	−6.2	Limestone clast	Section 4DC	
9B/NIMA	−0.6	−16.9	Limestone clast	Section 4DC	
9C/NIMA	−1.6	−18.3	Limestone clast	Section 4DC	
9D/NIMA	−2.5	−17.0	Limestone clast	Section 4DC	
9k/NIMA	−1.8	−16.1	Limestone clast	Section 4DC	
9G/NIMA	−0.3	−10.8	Limestone clast	Section 4DC	
9H/NIMA	0.3	−15.7	Limestone clast	Section 4DC	
9I/NIMA	−1.4	−16.4	Limestone clast	Section 4DC	
JQ 12B A1/JQ	1.9	−6.0	Limestone clast	Section 4DC	
JQ12B B /JQ	−2.8	−15.7	Limestone clast	Section 4DC	
JQ12B C /JQ	0.3	−9.9	Limestone clast	Section 4DC	
JQ-12B D1/JQ	−0.4	−14.8	Limestone clast	Section 4DC	
JQ-12B E1/JQ	2.4	−6.0	Limestone clast	Section 4DC	

shift that subsumes changes in the $\delta^{18}O$ values of seawater (~ + 0.4‰; [40]), increased global temperature (+6 °C, [40,41]), increased rainfall amount [11], and lower paleolatitude (~ 5° change or −0.6‰; [42]). Therefore, we added 2.5‰ to the $\delta^{18}O_{cc}$ values of paleosol carbonates for comparison purposes. Soil carbonate at soil depths >1.0 m forms at or near mean annual temperature, thus reducing the effects of diurnal and seasonal temperature fluctuations. To be conservative, we assign an additional ±5 °C uncertainty to the paleotemperature shift estimate in Fig. 4.

5. Oxygen and carbon isotope results

Texturally, the Lower Cretaceous limestone clasts are a mix of micrite and sparite and commonly contain obviously recrystallized marine fossils [43], whereas the Tertiary lacustrine marls and nodular paleosol carbonates are dense, well-indurated micrite containing well-preserved gastropod, ostracode, and *Chara* fossils. Analysis of the reworked Cretaceous marine limestone pebbles and cobbles yielded several $\delta^{18}O_{cc}$ values between −3‰ and −5‰ (Fig. 5; Table 2), in

Table 3
Analyses of modern soil carbonate from Nima area

Sample #	$\delta^{13}C$	$\delta^{18}O$	Depth	Elevation	GPS location		Description[1]
	PDB	PDB	(cm)	(m)	Longitude	Latitude	
NIMA 1 B	−0.5	−11.6	50	4495	45R 0537714	3515090	Stage I
NIMA 1 D	−3.2	−13.4	50	4495	45R 0537715	3515091	Stage I
NIMA 1 F	0.1	−11.7	50	4495	45R 0537716	3515092	Stage I
NIMA 1 H	−2.5	−13.0	50	4495	45R 0537717	3515093	Stage I
NIMA 4 A	−2.7	−13.8	120	4500	45R 0554041	3515591	Stage II
NIMA 4 B	7.7	−6.1	120	4500	45R 0554042	3515592	Stage II
NIMA 4 C	4.7	−9.1	120	4500	45R 0554043	3515593	Stage II
NIMA 4 D	2.3	−10.1	120	4500	45R 0554044	3515594	Stage II
NIMA 4 E	−2.0	−13.0	120	4500	45R 0554045	3515595	Stage II
NIMA 4 F	−3.4	−13.5	120	4500	45R 0554046	3515596	Stage II
NIMA 4 G	−1.8	−13.0	120	4500	45R 0554047	3515597	Stage II
NIMA 4 H	−2.5	−13.6	120	4500	45R 0554048	3515598	Stage II

[1]Soil development stage after Gile et al. [57].

the range expected for unaltered Cretaceous marine carbonates [44]. This indicates that some of the limestone pebbles are not diagenetically reset despite a long history of uplift, erosion, and at least two episodes of recycling over a time period of approximately 80 million years. Other Cretaceous limestone pebbles yielded $\delta^{18}O_{cc}$ values ranging between −5‰ and −15‰, suggesting that they have been diagenetically reset by interaction with meteoric waters (Fig. 5). However, the large spread in $\delta^{18}O_{cc}$ values of the marine limestone clasts, as contrasted with the tight clustering of Nima basin *in situ* and reworked paleosol carbonate $\delta^{18}O_{cc}$ values (Figs. 4, 5; Tables 1, 2) indicates that resetting must have occurred prior to deposition in the Nima basin, probably on now-eroded ancient outcrops or during previous burial events prior to erosion and final deposition in the Nima basin during the middle Tertiary. Therefore, the isotopic data that we report from paleosol carbonate and marl in the Nima basin may be interpreted to accurately represent the original isotopic composition of meteoric water during the Late Oligocene.

Paleosol carbonate nodules in Nima basin yielded $\delta^{18}O_{cc}$ values (Table 1) that average −17.0±0.3‰ (range −16.3 to −17.5‰; n=31) and $\delta^{13}C_{cc}$ values with an average of −3.5±0.6‰ (range −2.3 to −4.6‰). Our analyses include both nodules *in situ* within paleosols and nodules that were locally reworked into fluvial channels soon after formation (Figs. 4, 5); $\delta^{18}O_{cc}$ and $\delta^{13}C_{cc}$ values for both are identical. Minor corrections for a warmer Earth, decreased Cenozoic ice volume, and lower latitude at 26 Ma yield a mean paleosol carbonate $\delta^{18}O_{cc}$ value for Nima basin of −14.4‰. Corresponding correction for temperature of carbon isotopic values shifts the mean $\delta^{13}C_{cc}$ value to −2.9‰ (Fig. 4).

For comparison, modern soil carbonate in the Nima area (12 analyses from three local soil profiles; Table 3) at 4500 m elevation ranges from −13.8‰ to −6.1‰ for $\delta^{18}O_{cc}$ (Fig. 4). Meteoric water samples from springs

Table 4
Analyses of modern waters in the Nima basin

Sample #	Sample elevation	$\delta^{18}O$	δH	GPS location		Description
	(m)	(SMOW)	(SMOW)	Longitude	Latitude	
H2OJQ-44	4811	−14.2	−103	44R 430417	3478283	Small creek
H2OJQ-45	4836	−14.1	−97	44R 493102	3457492	Small creek
H2OJQ-46	4582	−16.2	−119	44R 498795	3445387	Medium creek
H2OJQ-48	4909	−15.0	−111	44R 595660	3410400	Small creek
H2OJQ-49	4806	−14.5	−109	44R 730405	3539677	Small creek
H2OJQ-50	4265	−13.0	−118	44R 751505	3545191	Major river
H2OJQ-51	4488	−15.8	−125	44R 760476	3541874	Small creek
H2OJQ-52	4592	−14.9	−117	46R 236676	3484214	Small creek
H2OJQ-53	4621	−12.6	−93	46R 296274	3435950	Medium creek

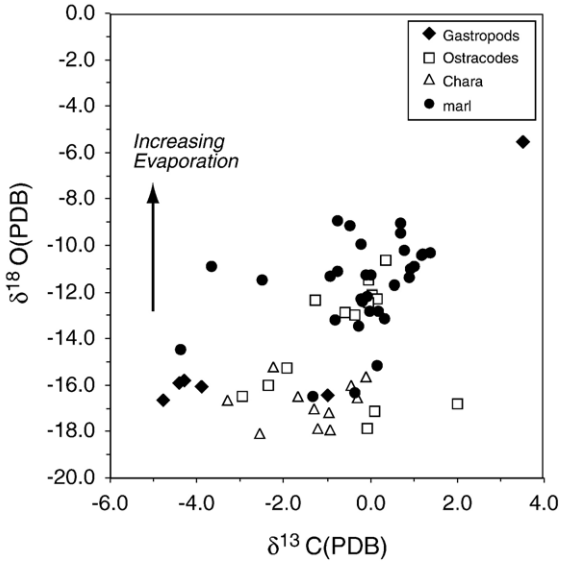

Fig. 6. $\delta^{18}O$ (PDB) versus $\delta^{13}C$ (PDB) of Late Oligocene fossils from Nima basin. Fossils were collected from micritic marl beds and sampled by microdrilling.

and small creeks in the Nima area at modern elevations of 4500–5000 m yielded $\delta^{18}O_{mw}$ values that range from −12.6‰ to −16.2‰ (Table 4; J. Quade, unpublished data). $\delta^{18}O_{cc}$ of soil carbonate forming in isotopic equilibrium with these waters should be −11.7 to −13.3‰, assuming local mean annual temperature of 3 °C [45]. Modern soil carbonate $\delta^{18}O_{cc}$ values (−13.8 to −6.1‰) fully overlap the predicted range (−11.7 to −13.3‰) but also exhibit much more positive values. This shows that much of, but not all, modern soil water is highly evaporated compared to rainfall prior to soil carbonate formation, which is consistent with the modern arid setting of Nima basin (annual rainfall is ~ 200 mm/yr). The most negative (least evaporated) $\delta^{18}O_{cc}$ value of −13.8‰ for modern soil carbonate is comparable to the corrected $\delta^{18}O_{cc}$ values from Nima paleosol carbonates of −14.4‰. However, owing to possible evaporation in paleosol water, paleo-$\delta^{18}O_{mw}$ may have been lower, and paleoelevation correspondingly higher. Thus, from the oxygen isotope perspective, the elevation of the Nima basin sample sites (4500–4700 m) was at least as high during the Late Oligocene.

The carbon isotope results support this picture of uniformity. Modern soil carbonates yielded $\delta^{13}C_{cc}$ values in the −3.4 to +7.7‰ range (Fig. 4; Table 3). The $\delta^{13}C_{cc}$ value of soil carbonate is determined by the local proportion of C_3 to C_4 plants, and, where conditions are dry, by the extent of local plant cover [46]. Our analyses show that almost all of the local plants are C_3 (Table 5); thus, the $\delta^{13}C_{cc}$ values can be used to interpret paleorespiration rates, provided atmospheric pCO_2 has not changed substantially [47]. The relatively high $\delta^{13}C_{cc}$ values for modern soils clearly point to mixing of atmospheric CO_2 with plant-derived CO_2 owing to low soil respiration rates, again the result of the arid local climate. Temperature-corrected $\delta^{13}C_{cc}$ values of −2.9‰ from paleosols in the Nima area also indicate very low soil respiration rates at 26–25 Ma (Fig. 4). Modern and ancient soil respiration rates of 0.3 to 0.4 mmol/m^2/h can be calculated from the one-dimensional soil diffusion model of [48] and modified in [46], assuming −25‰ is the average $\delta^{13}C$ value of plants (determined from our analysis of local plants; Table 5), mean annual temperature of 2.9 °C, pCO_2 <500 ppm [47], and an average $\delta^{13}C_{cc}$ value of −2.9‰. These respiration rates are very low and typical of sparsely vegetated desert settings in North America [46] that receive less than ~ 200 mm/yr of annual rainfall. Aridity in modern Tibet is produced by orographic blockage of moisture arriving from outside the plateau, as well as by orographically induced stationary waves that tend to fix dry, descending air over the plateau during most of the year [36]. The implication of the high $\delta^{13}C_{cc}$ values from Nima basin paleosols is that orographic barriers to moisture also existed during the Late Oligocene. The most likely location of these orographic barriers is in the Himalaya, which was actively growing during Oligocene time and earlier (see summary in [49]).

Analyses of samples of Nima basin fossils and marls provide additional information about the paleoelevation of Nima basin (Table 6; Fig. 6). The marls are micritic and massive to delicately laminated, and locally contain abundant ostracodes, mollusks, and *Chara* that appear petrologically and geochemically unaltered. Small samples of fresh micritic marl from lacustrine intervals throughout the section yielded $\delta^{18}O_{cc}$ values ranging between −8.9 and −16.5 (Table 6). Analysis of microsamples of freshwater aquatic fossils and associated matrix produced $\delta^{18}O_{cc}$ values of −4.7 to −18.1‰ (Fig. 6, Table 6). Values of $\delta^{18}O_{cc}$ from individual growth laminae in gastropod shells range between −15.8‰ and −16.7‰. The most negative of these $\delta^{18}O_{cc}$ values are consistent with similarly low values from paleosol carbonates in the section, indicating high elevations of catchment areas surrounding the Nima basin. Moreover, the large spread of $\delta^{18}O_{cc}$ values (−4.7 to −18.1) in lacustrine micrite and fossils suggests substantial evaporation, the same pattern seen in modern high-elevation lakes in Tibet, where $\delta^{18}O_{mw}$ values are strongly increased by evaporation [50]. Other evidence

in the Nima basin deposits also supports the view of a high and dry setting during the Late Oligocene. Evaporites and mudcracks are common throughout the stratigraphic succession, and eolian dune deposits are common in palynologically dated Upper Cretaceous deposits in the northern part of Nima basin [35].

6. Discussion

A key imponderable in any reconstruction of paleoelevation using oxygen isotopes–especially in deep time such as this case — is climate change related to such factors as major air-mass reorganizations. As an example, we noted in the Introduction that from the perspective of oxygen isotopes, Tibet can be divided into two regions: a southern region, including the Nima and Lunpola basins, where oxygen isotope lapse rates are steep (−2.8‰/km) and $\delta^{18}O_{mw}$ values for mean annual rainfall are very negative (−15 to −20‰), and a northern region, including Xoh Xil, where lapse rates are half those of the south and the lowest $\delta^{18}O_{mw}$ values are around −8 to −10‰ [28, 29]. These isotopic contrasts reflect the sharp climate divisions of modern Tibet, between a monsoon-dominated south and the more interior air mass-dominated north. This is an important caveat for those interested in paleoelevation reconstruction using $\delta^{18}O_{cc}$ values, and reminds us of the fundamental role that climate plays in determining lapse rates.

The question is: How might changes in past climate and orography affect our paleoelevation reconstruction for Nima during the Late Oligocene? The answer is that several plausible scenarios would make our paleoelevation estimate for the Nima basin a minimum, whereas no realistic scenario would make it an overestimate. One obvious possibility is that the boundary between southerly and northerly air masses, now positioned well to the north of Nima, was farther south at 26 Ma, the result of, for example, a weaker Asian Monsoon. In this case, the lower lapse rates characteristic of northern Tibet today would apply to Nima, sharply increasing, not decreasing our estimate of paleoelevation. A second interesting possibility is that the Himalaya to the south was topographically subdued during the Late Oligocene. Lower mountains to the south would have reduced the average amount of rain-out from tropical moisture parcels as they moved northward, thus lowering the isotopic lapse rate and increasing the average $\delta^{18}O_{mw}$ values of precipitation falling on southern Tibet. Again, this would tend to make our estimate of paleoelevation a minimum. The only reasonable way for our paleoelevation estimate to be an overestimate would be for the paleolapse rate to have been greater, a situation that could have existed if the region was significantly cooler than today or if the Oligocene Himalaya was much higher than it is today. Significantly cooler regional temperatures would increase rain-out from air masses due to enhanced condensation (similar to winter precipitation in temperate climates), leading to more negative $\delta^{18}O_{mw}$ values and a greater isotopic lapse rate. However, given the Cenozoic history of cooling since the Eocene, it is much more likely that temperatures were warmer than today at 26 Ma in the Nima Basin. Although geological records of Himalayan thrusting and erosional unroofing have not, to date, been shown to be consistent with a diminishing Himalaya since the Late Oligocene [14,51,52], these hypotheses remain largely untested. A decline in elevation in the Himalaya since Middle Miocene could be consistent with widespread north-striking normal faults and Late Miocene extensional basins in southern Tibet and the northern Himalayan thrust belt [49,53]. In any case, this analysis underscores the basic observation that $\delta^{18}O_{mw}$ values in the Himalaya and southern Tibet today are much more negative than in any other low to mid-latitude setting. In essence, we have no other modern setting in which $\delta^{18}O_{mw}$ values are as negative as they are today at these latitudes and elevations.

Further work is needed to test the conclusions that we draw from an admittedly limited data set, which is derived from a local region over a brief timespan (only a few million years). Given the data we have in hand from both modern and Late Oligocene Tibet, the conservative view is that no significant elevation change has occurred in central Tibet since ~ 26 Ma. This conclusion is consistent with recent findings based on palynologically dated Eocene deposits in Lunpola basin [23], but in our view more data are required from securely dated Tertiary basin fills all across Tibet before a regional progression of elevation gain, such as that proposed by [23,32], is demonstrated. Existing paleoelevation data in Tibet come from only a handful of sites spread across a region roughly half the size of the United States [12,23,54]. Our results do not preclude even earlier attainment of high elevation in central and southern Tibet, where Late Cretaceous–Paleocene crustal shortening was significant (>40–50%), erosional denudation was minimal, and development of a significant fraction of the present-day crustal thickness (~ 70 km) could have produced high regional elevation before the Indo–Asian collision [30,55]. Like the results from Lunpola basin [23], our data are not consistent with models that call for significant uplift of the entire Tibetan Plateau during Late Miocene or Pliocene time [1,56], but we cannot

eliminate the possibility that the region north of Nima experienced significant surface uplift after the Late Oligocene. If we accept the palynological ages from Lunpola basin at face value, one could argue that the northern Lhasa terrane had achieved a high (>4 km) elevation by late Middle Eocene time (ca. 39 Ma according to [23]) and that this elevation remained constant through Late Oligocene to the present. This is consistent with models that suggest that the elevation of the Plateau interior reached a maximum value and subsequently remained constant while the Plateau expanded laterally [2]. In any case, the maintenance of uniform elevation in the central part of the Plateau since at least the Late Oligocene requires that any flow of lower crust from beneath central Tibet [2,5] must have been balanced by an influx of lower crust from elsewhere. It is plausible that central Tibetan crust was largely thickened and at least partly elevated during shortening prior to the Indo–Asian collision [6,30,55], and that the volume of central Tibetan lower crust removed by subduction [4] and/or eastward flow to uplift the eastern Tibetan Plateau [2,5] was balanced and partly driven by the northward insertion of Indian crust along the Himalayan margin [3,7,8].

7. Conclusions

Comparison of oxygen isotope ratios in well-dated paleosol carbonates with ratios from modern soils in central Tibet indicates that paleoelevation was ~ 4500–5000 m during Late Oligocene time. Oxygen isotope ratios in unaltered aquatic fossils also support the conclusion that the Nima basin has been at high elevation since the Late Oligocene. Oxygen isotope ratios from Oligocene lacustrine marl and $\delta^{13}C_{mw}$ values from paleosol carbonate indicate high rates of evaporation and low soil respiration rates, respectively, both consistent with arid paleoclimate. Abundant arid-climate lithofacies, including evaporites and eolian deposits, indicate that this part of Tibet has been arid since Late Cretaceous time. Thus the present elevation and climatic conditions in central Tibet have not changed significantly since at least as long ago as the Late Oligocene. The presence of thickened crust in central Tibet by Late Oligocene, and perhaps even Late Cretaceous, time can be reasonably inferred on the basis of regional crustal shortening estimates (~ 50%). Underthrusting Indian crust and lithosphere beneath the Tibetan Plateau since Eocene time most likely would have encountered previously thickened Tibetan lower crust and would have driven east-southeastward crustal flow into marginal regions.

Acknowledgments

We thank Shiling Yang for the assistance in the laboratory, and B. Quade and E. Quade for the assistance in the field. Research was supported by the National Science Foundation and ExxonMobil Corporation. We thank Brad Ritts, Page Chamberlain, and Peggy Delaney for the constructive reviews that helped us to substantially improve this manuscript.

Appendix A. Supplementary data

Supplementary data associated with this article can be found, in the online version, at doi:10.1016/j.epsl.2006.11.001.

References

[1] P. Molnar, P. England, J. Martinod, Mantle dynamics, uplift of the Tibetan Plateau, and the Indian Monsoon, Rev. Geophys. 31 (1993) 357–396.
[2] L.H. Royden, B.C. Burchfiel, R.W. King, E. Wang, Z. Chen, et al., Surface deformation and lower crustal flow in eastern Tibet, Science 276 (1997) 788–790.
[3] W. Zhao, W.J. Morgan, Injection of Indian crust into Tibetan lower crust: a two-dimensional finite element model study, Tectonics 6 (1987) 489–504.
[4] P. Tapponnier, X. Zhiqin, F. Roger, B. Meyer, N. Arnaud, G. Wittlinger, Y. Jingsui, Oblique stepwise rise and growth of the Tibet Plateau, Science 294 (2001) 1671–1677.
[5] M.K. Clark, L.H. Royden, Topographic ooze: building the eastern margin of Tibet by lower crustal flow, Geology 28 (2000) 703–706.
[6] A. Yin, T.M. Harrison, Geologic evolution of the Himalayan–Tibetan orogen, Annu. Rev. Earth Planet. Sci. 28 (2000) 211–280.
[7] P.G. DeCelles, D.M. Robinson, G. Zandt, 2002, implications of shortening in the Himalayan fold-thrust belt for uplift of the Tibetan Plateau, Tectonics 21 (2002) 1062, doi:10.1029/2001TC001322.
[8] C. Beaumont, R.A. Jamieson, M.H. Nguyen, B. Lee, Himalayan tectonics explained by extrusion of a low-viscosity crustal channel coupled to focused surface denudation, Nature 414 (2001) 738–742.
[9] W.F. Ruddiman, J.E. Kutzbach, Forcing of late Cenozoic Northern Hemisphere climate by plateau uplift in southern Asia and the American west, J. Geophys. Res. 94 (D15) (1989) 18,409–18,427.
[10] W.L. Prell, J.E. Kutzbach, Sensitivity of the Indian monsoon to forcing parameters and implications for its evolution, Nature 360 (1992) 647–652.
[11] J. Quade, J.M.L. Cater, T.P. Ojha, J. Adam, T.M. Harrison, Late Miocene environmental change in Nepal and the northern Indian subcontinent: stable isotopic evidence from paleosols, Geol. Soc. Amer. Bull. 107 (1995) 1381–1397.
[12] P.M. Blisniuk, L.A. Stern, Stable isotope paleoaltimetry: a critical review, Am. J. Sci. 305 (2005) 1033–1074.
[13] C.N. Garzione, J. Quade, P.G. DeCelles, N.B. English, Predicting paleoelevation of Tibet and the Nepal Himalaya from $\partial^{18}O$ vs. altitude gradients in meteoric water across the

Nepal Himalaya, Earth Planet. Sci. Lett. 183 (2000) 215–230.
[14] C.N. Garzione, D.L. Dettman, J. Quade, P.G. DeCelles, R.F. Butler, High times on the Tibetan Plateau: paleoelevation of the Thakkhola graben, Nepal, Geology 28 (2000) 339–342.
[15] D.L. Dettman, K.C. Lohmann, Oxygen isotope evidence for high altitude snow in the Laramide Rocky Mountains of North America during the late Cretaceous and Paleogene, Geology 28 (2000) 243–246.
[16] C.N. Garzione, P. Molnar, J.C. Libarkin, B.J. MacFadden, Rapid Late Miocene rise of the Bolivian Altiplano: evidence for removal of mantle lithosphere, Earth Planet. Sci. Lett. 241 (2006) 543–556.
[17] M.A. Poage, C.P. Chamberlain, Empirical relationships between elevation and the stable isotope composition of precipitation and surface waters: considerations for studies of paleoelevation change, Am. J. Sci. 301 (2001) 1–15.
[18] D.B. Rowley, R.T. Pierrehumbert, B.S. Currie, A new approach to stable isotope-based paleoaltimetry: implications for paleoaltimetry and paleohypsometry of the High Himalaya since the Late Miocene, Earth Planet. Sci. Lett. 188 (2001) 253–268.
[19] D.L. Dettman, X. Fang, C.N. Garzione, J. Li, Uplift-driven climate change at 12 Ma: a long $\delta^{18}O$ record from the NE margin of the Tibetan plateau, Earth Planet. Sci. Lett. 214 (2003) 267–277.
[20] A. Mulch, C. Teyssier, M.A. Cosca, O. Vanderhaeghe, T. Vennemann, Reconstructing paleoelevation in eroded orogens, Geology 32 (2004) 525–528.
[21] A.J. Cyr, B.S. Currie, D.B. Rowley, Geochemical evaluation of Fenghuoshan Group lacustrine carbonates, north-central Tibet: implications for the paleoaltimetry of the Eocene Tibetan Plateau, J. Geol. 113 (2005) 517–533.
[22] B.S. Currie, D.B. Rowley, N.J. Tabor, Middle Miocene paleoaltimetry of southern Tibet: implications for the role of mantle thickening and delamination in the Himalayan orogen, Geology 33 (2005) 181–184.
[23] D.B. Rowley, B.S. Currie, Palaeo-altimetry of the late Eocene to Miocene Lunpola basin, central Tibet, Nature 439 (2006) 677–681.
[24] S.A. Graham, C.P. Chamberlain, Y. Yue, B.D. Ritts, A.D. Hanson, T.W. Horton, J.R. Waldbauer, M.A. Poage, X. Feng, Stable isotope records of Cenozoic climate and topography, Tibetan Plateau and Tarim basin, Am. J. Sci. 305 (2005) 101–118.
[25] T.W. Horton, D.J. Sjostrom, M.J. Abruzzese, M.A. Poage, J.R. Waldbauer, M. Hren, J. Wooden, C.P. Chamberlain, Spatial and temporal variation of Cenozoic surface elevation in the Great Basin and Sierra Nevada, Am. J. Sci. 304 (2004) 862–888.
[26] M.L. Kent-Corson, L.S. Sherman, A. Mulch, C.P. Chamberlain, Cenozoic Topographic and Climatic Response to Changing Tectonic Boundary Conditions in Western North America, Earth Planet. Sci. Lett. (2006), doi:10.1016/j.epsl.2006.09.049.
[27] R. Spicer, N. Harris, M. Widdowson, A. Herman, S. Guo, P. Valdes, J. Wolf, S. Kelley, Constant elevation of southern Tibet over the past 15 million years, Nature 421 (2003) 622–624.
[28] L. Tian, V. Masson-Delmotte, M. Stievenard, T. Yao, J. Jouzel, Tibetan plateau summer monsoon northward extent revealed by measurements of water stable isotopes, J. Geophys. Res. 106 (D22) (2001) 28,081–28,088.
[29] L. Araguas-Araguas, K. Froehlich, K. Rozanski, Stable isotope composition of precipitation over Southeast Asia, J. Geophys. Res. 103 (1998) 28721–28742.
[30] P. Kapp, A. Yin, T.M. Harrison, L. Ding, Cretaceous–Tertiary shortening, basin development, and volcanism in central Tibet, Geol. Soc. Amer. Bull. 117 (2005) 865–878.
[31] B.K. Horton, A. Yin, M.S. Spurlin, J. Zhou, J. Wang, Paleocene–Eocene syncontractional sedimentation in narrow, lacustrine-dominated basins of east-central Tibet, Geol. Soc. Amer. Bull. 114 (2002) 771–786.
[32] A. Mulch, C.P. Chamberlain, The rise and growth of Tibet, Nature 439 (2006) 670–671.
[33] P.G. DeCelles, P. Kapp, J. Quade, M. Fan, High and dry: central Tibetan Plateau during the mid-Tertiary, Eos Trans. AGU 86 (2005) (Fall Meet. Suppl.).
[34] P. Kapp, P.G. DeCelles, G.E. Gehrels, M. Heizler, L. Ding, Geological records of the Lhasa–Qiangtang and Indo–Asian collisions in the Nima area of central Tibet, Geol. Soc. Amer. Bull. (submitted for publication).
[35] P.G. DeCelles, P. Kapp, L. Ding, G.E. Gehrels, Late Cretaceous to mid-Tertiary basin evolution in the central Tibetan Plateau: Changing environments in response to tectonic partitioning, aridification, and regional elevation gain, Geol. Soc. Amer. Bull. (in press).
[36] A.J. Broccoli, S. Manabe, The effects of orography on midlatitude Northern Hemisphere dry climates, J. Climate 5 (1992) 1181–1201.
[37] C.N. Garzione, D.L. Dettman, B.K. Horton, Carbonate oxygen isotope paleoaltimetry: evaluating the effect of diagenesis on paleoelevation estimates for the Tibetan plateau, Palaeogeogr. Palaeoclimatol. Palaeoecol. 212 (2004) 119–140.
[38] R.F. Butler, Paleomagnetism, Blackwell Scientific, Boston, 1992.
[39] G.H. Mack, W. Calvin James, H. Curtis Monger, Classification of paleosols, Geol. Soc. Amer. Bull. 105 (1993) 129–136.
[40] J.C. Zachos, L.D. Stott, K.C. Lohmann, Evolution of marine temperatures during the Paleogene, Paleoceanography 9 (1994) 353–387.
[41] N.J. Shackleton, J.P. Kennett, in: J.P. Kennett, R. Houtz (Eds.), Paleotemperature History of the Cenozoic and the Initiation of Antarctic Glaciation: Oxygen and Carbon Isotope Analyses in DSDP Sites 277, 279, and 281, Initial Report of Deep Sea Drilling Project Leg, vol. 29, 1975, pp. 743–955.
[42] G.J. Bowen, B. Wilkinson, Spatial distribution of $\delta^{18}O$ in meteoric precipitation, Geology 30 (2002) 315–318.
[43] A.L. Leier, The Cretaceous evolution of the Lhasa terrane, southern Tibet, Ph.D. Dissertation, Univ. of Arizona, 2005.
[44] J. Veizer, D. Ala, K. Azmy, P. Bruckschen, D. Buhla, F. Bruhn, G.A.F. Carden, A. Diener, S. Ebneth, Y. Godderis, T. Jasper, C. Korte, F. Pawellek, O.G. Podlaha, H. Strauss, $^{87}Sr/^{86}Sr$, $\delta^{13}C$ and $\delta^{18}O$ evolution of Phanerozoic seawater, Chem. Geol. 161 (1999) 59–88.
[45] S.-T. Kim, J.R. O'Neil, Equilibrium and nonequilibrium oxygen isotope effects in synthetic carbonates, Geochim. Cosmochim. Acta 61 (1997) 3461–3475.
[46] J. Quade, T.E. Cerling, J. Bowman, Development of Asian monsoon revealed by marked ecological shift during latest Miocene in northern Pakistan, Nature 342 (1989) 163–166, doi:10.1038/342163a0.
[47] M. Pagani, J. Zachos, K.H. Freeman, B. Tipple, S. Bohaty, Marked decline in atmospheric carbon dioxide concentrations during the Paleogene, Science 309 (2005) 600–603.
[48] T.E. Cerling, The stable isotopic composition of modern soil carbonate and its relationship to climate, Earth Planet. Sci. Lett. 71 (1984) 229–240.

[49] K.V. Hodges, Tectonics of the Himalaya and southern Tibet from two perspectives, Geol. Soc. Amer. Bull. 112 (2000) 324–350.
[50] F. Gasse, J.Ch. Fontes, E. Van Campo, K. Wei, Holocene environmental changes in Bangong Co basin (western Tibet). Part 4: discussion and conclusions, Palaeogeogr. Palaeoclimatol. Palaeoecol. 120 (1996) 79–92.
[51] P.G. DeCelles, G.E. Gehrels, Y. Najman, A.J. Martin, A. Carter, E. Garzanti, Detrital geochronology and geochemistry of Cretaceous–early Miocene strata of Nepal: implications for timing and diachroneity of initial Himalayan orogenesis, Earth Planet. Sci. Lett. 227 (2004) 313–330.
[52] Y. Najman, The detrital record of orogenesis: a review of approaches and techniques used in the Himalayan sedimentary basins, Earth-Sci. Rev. (2006) 1–72.
[53] P. Kapp, J.H. Guynn, Indian punch rifts Tibet, Geology 32 (2004) 993–996.
[54] N. Harris, The elevation history of the Tibetan Plateau and its implications for the Asian monsoon, Palaeogeogr. Palaeoclimatol. Palaeoecol. 241 (2006) 4–15.
[55] M.A. Murphy, A. Yin, T.M. Garrison, S.B. Durr, Z. Chen, F.J. Ryerson, W.S.F. Kidd, X Wang, X. Zhou, Did the Indo–Asian collision alone create the Tibetan plateau? Geology 25 (1997) 719–722.
[56] Y. Wang, T. Deng, D. Biasatti, Ancient diets indicate significant uplift of southern Tibet after ca. 7 Ma, Geology 34 (2006) 309–312.
[57] L.H. Gile, F.F. Peterson, R.B. Grossman, Morphological and genetic sequences of carbonate accumulation in desert soils, Soil Sci. 101 (1966) 347–360.